Radially Periodic Leaky-Wave Antenna for Bessel-Beam Generation over a Wide Frequency Range

Davide Comite, *Member, IEEE,* Walter Fuscaldo, *Student Member, IEEE,* Symon K. Podilchak, *Member, IEEE,* Pascual D. Hilario Re, *Student Member, IEEE,* Victoria Gómez-Guillamón Buendía, *Student Member, IEEE,* Paolo Burghignoli, *Senior Member, IEEE,* Paolo Baccarelli, *Member, IEEE,* and Alessandro Galli, *Member, IEEE*

***Abstract*—A radially periodic two-dimensional leaky-wave antenna is studied for the generation of zeroth-order Bessel beams within a limited spatial region and over a wide frequency range. The antenna design is wideband and based on an annular metal strip grating placed on top of a grounded dielectric slab, supporting a cylindrical leaky wave with a fast *backward* spatial harmonic. The focusing capabilities of the relevant leaky-wave aperture fields are investigated over the considered frequency range (15 to 21 GHz), in conjunction with the dispersion analysis of the optimized structure, which is developed by means of an efficient in-house method-of-moments code. Full-wave simulations using a commercial tool including a simple coaxial feeder are presented and discussed, demonstrating the desired wideband operation. The antenna design is validated by means of measurements performed on a manufactured prototype, considering different frequencies and components of the electric field within the nondiffracting range of the system. The proposed design represents an attractive simple and low-cost solution potentially able to generate arbitrary-order Bessel beams at microwaves as well as in the millimeter-wave and terahertz frequency regions.**

***Index Terms*—Bessel beams, nondiffracting waves, leaky waves, near-field, backward spatial harmonics, metallic strip grating.**

I. Introduction and Motivation

DIFFRACTION is a well-recognized physical phenomenon that prevents the possibility of focusing the radiation by an aperture over arbitrary distances. Ideal nondiffracting solutions of the scalar wave equation are the so-called Bessel beams [1], [2], whose amplitude transverse profile is described by an nth-order Bessel function. As originally demonstrated in [1], a Bessel beam can rigorously be excited only by transversely unbounded apertures, which would require an infinite amount of energy to be illuminated. However, the nondiffracting (i.e., collimated) behavior of such a beam can still be obtained with a truncated aperture inside a *limited* region in the near-field, within a distance known as *nondiffracting range* (NDR) [1]. Up to the NDR the transverse profile of the beam is accurately described by the relevant Bessel function, whereas beyond the NDR the agreement with such a function gradually deteriorates and the beam loses its collimated near-field behavior.

In the last few decades, several works have discussed the possibility of generating Bessel beams. Many designs have been proposed (see, e.g., [3]-[17], and references therein). In the microwave frequency region, an experimental generation of a zeroth-order Bessel beam was given in [11], where the authors proposed a practical solution to synthesize collimated fields by means of a finite aperture using leaky-wave (LW) modes supported by a cylindrical resonant structure. The launcher benefits by the design of a simple feeding system, but operates in a narrow fractional bandwidth, mainly due to the resonant nature of the relevant aperture distribution. Radial line slotted array (RLSA) antennas, designed through holographic principles, have also been proposed in [14] and [15]. A millimeter-wave launcher based on a similar resonant structure as in [11], but exploiting higher-oder leaky modes, has been designed and validated in [17] over a 4% fractional bandwidth.

The possibility of generating collimated beams by means of an inward traveling wave aperture distribution has been theoretically studied in [18] and experimentally demonstrated in [19] with an RLSA design operating from about 12.2 GHz to 12.7 GHz, resulting in the generation of a Bessel beam over a narrow frequency range. A radial waveguide designed through a holographic technique was also proposed in [20], supporting a 6.5% fractional bandwidth around 30 GHz. In [21], the capability of the RLSA to excite higher-order (i.e., vortex) Bessel beams has been examined from 11.5 GHz to 13.5 GHz. This corresponds to a fractional bandwidth of about 16%. An alternative design to generate a vortex beam based on a transmitarray approach has also been recently presented in [22] at 10 GHz. A metamaterial lens was designed in [23] with a fractional bandwidth of 40% around 15 GHz, but resulting in a bulky and non-planar structure. Finally, a reflectarray was used in [24] to generate a Bessel beam from 27 GHz to 31 GHz, defining a fractional bandwidth of 13.8%.

Following these developments, the backward LW radiation supported by a holographic metasurface has been exploited in [25] to realize a zeroth-order Bessel beam from 16.5 GHz to 17.5 GHz. On the other hand, backward LWs have also

Davide Comite, Walter Fuscaldo, Paolo Burghignoli, and Alessandro Galli are with the Department of Information Engineering, Electronics and Telecommunications, "Sapienza" University of Rome, 00184 Rome, Italy (e-mail: davide.comite@uniroma1.it).

Paolo Baccarelli is with the Department of Engineering, "Roma Tre" University, 00146 Rome, Italy (e-mail: paolo.baccarelli@uniroma3.it).

Pascual D. Hilario Re, Victoria Gómez-Guillamón Buendía, and Symon K. Podilchak are with the Institute of Sensors, Signals, and Systems, School of Engineering and Physical Sciences Edinburgh Campus, Heriot-Watt University, Edinburgh EH14 4AS, United Kindom, (email: s.podilchak@hw.ac.uk).

Manuscript received September 14th, 2017. Accepted March 30th, 2018.

been successfully exploited to design LW lenses [26]-[28], where a focused field was achieved inside the Fresnel region for the considered radiator. In particular, a spiral arrangement of unit cells supporting an $m = -1$ fast spatial harmonic was described and measured in [27], whereas a non-uniform sinusoidally modulated half-mode microstrip structure was designed in [28] and arranged in an annular configuration.

In this paper, we demonstrate theoretically and experimentally that a nondiffracting or collimated beam can be also generated through a more conventional radially periodic two-dimensional (2-D) leaky-wave antenna (LWA) [29]. A so-called 'bull-eye' structure is designed (see Fig. 1), similar to those proposed, e.g., in [30]-[32], in single- and dual-layer configurations. Furthermore, the experimental validation of our LWA examined in this work for Bessel beam generation in the near-field, allows us to demonstrate that the LW mode supported by such an annular 2-D structure can effectively be modeled using a Method of Moments (MoM) dispersive analysis for a corresponding 1-D linearized structure [30]-[32]. This is an essential aspect in the design, since, due to the non-translational invariance of the annular geometry, other modeling approaches found in the literature are limited when considering this class of radially periodic LWA.

Regardless, this type of low-cost planar antenna is simple to feed and can be made by an annular arrangement of metallic strips placed on a grounded dielectric slab (GDS) and can indeed support backward LWs. This aperture-field distribution can synthesize an inward traveling wave over a significantly wide bandwidth, here designed from 14 GHz to more than 21 GHz. This defines a fractional bandwidth of about 40%. If properly excited, the backward LW can propagate radially and leak more than 90% of the injected power for radiation before reaching the aperture truncation, thus describing the cylindrical aperture-field distribution [33], which, as discussed in [18], is required to synthesize a focused beam propagating along the axis of symmetry of the structure.

Our antenna furthermore, as fully described in this paper, is an alternative to the design originally proposed in [10] based on forward LWs, which shows that a Bessel-like aperture distribution can be generated as a superposition of an outward and an inward Hankel wave. This was obtained in [10] by exciting an outward forward leaky mode in a radial waveguide, which is reflected back by a circular metallic rim properly positioned at a particular radial distance to recover the desired inward character. This method of generating Bessel beams is inherently narrow-band since it is based on the resonant-like character of the leaky field generated on the aperture. Conversely, in our design, the backward LW is unaffected by the truncation when the aperture length is sufficiently large. We also stress that the top aperture of the structure in [10] and [11] is constituted by a homogenizable capacitive impedance sheet, which is in practice made by a double-layer of square patches (i.e., printed on both sides of an electrically-thin substrate) [11]. Hence, this structure radiates via the fundamental Floquet harmonic (i.e., $m = 0$).

On the other hand, the LWA proposed in this paper operates by radiation of the $m = -1$ spatial harmonic and represents a possible alternative to more established RLSA antennas [15], [19], [21], [34], resulting in simple synthesis and manufacturing processes (for the microwave frequency range and beyond). In fact, our structure also operates in a wide frequency band, and does not require a full-wave optimization procedure to design the RLSA slot layout needed to synthesize the desired aperture-field distribution as in some previous works. In addition, by properly designing the feed system, and using the same planar configuration and strip arrangement, as proposed in this work, we can potentially generate arbitrary orders of nondiffracting Bessel beams having nth-order azimuthal phase variations. This is of interest for several applications, such as, e.g., enhanced communications and buried-object detection [35], [36].

We finally mention that a preliminary LW antenna design supporting an inward traveling wave, excited by an ideal source, has been reported by the authors in [37]. However, we propose, analyze, and experimentally characterize in this paper a completely new and wideband design. The antenna structure is excited by a simple and practical source and supported by a commercially available PCB material. In addition, a new and optimized geometry for the unit cell, defined by the top metallic strip grating (MSG), is fully examined in this paper using LW theory and a MoM dispersion analysis.

This paper is organized as follows. Sec. II presents the main theoretical background regarding the aperture field distribution needed to synthesize collimated beams in the near-field, whereas Sec. III presents the design of the antenna in conjunction with the relevant dispersive analysis. Sec. IV reports the results obtained by simulating the wideband antenna using a commercial full-wave tool and considering a practical and simple to implement feed system. Experimental results obtained through measurements of a manufactured prototype are presented in Sec. V and some conclusions are drawn in Sec. VI.

II. Theoretical Background

We consider in this section a vectorial formulation for an nth-order Bessel beam, assuming and suppressing a time dependence of the kind $e^{j\omega t}$. Without loss of generality we refer to an nth-order Bessel beam propagating along the vertical z-axis, with transverse-magnetic (TM) polarization with respect to z. In a cylindrical coordinate system (ρ, ϕ, z), the electric-field components of the Bessel beam are

$$E_z(\rho,\phi,z) = E_0 J_n(k_\rho \rho) e^{-jn\phi} e^{-jk_z z} \tag{1}$$

$$E_\rho(\rho,\phi,z) = -j\frac{k_z}{k_\rho} E_0 J_n'(k_\rho \rho) e^{-jn\phi} e^{-jk_z z} \tag{2}$$

$$E_\phi(\rho,\phi,z) = -\frac{nk_z}{k_\rho^2} E_0 \frac{J_n(k_\rho \rho)}{\rho} e^{-jn\phi} e^{-jk_z z} \tag{3}$$

where $J_n(\cdot)$ is the nth-order Bessel function of the first kind, $J_n'(\cdot)$ is the first-order derivative of the same function, k_ρ and $k_z = (k_0^2 - k_\rho)^{1/2}$ are the transverse and vertical wavenumbers associated with the beam; k_0 is the free-space wavenumber and E_0 is a complex constant amplitude factor depending on the excitation. If $n = 0$, a zeroth-order azimuthally symmetric beam is generated, while for $n \neq 0$ an nth-order beam with an azimuthal phase variation can be observed.

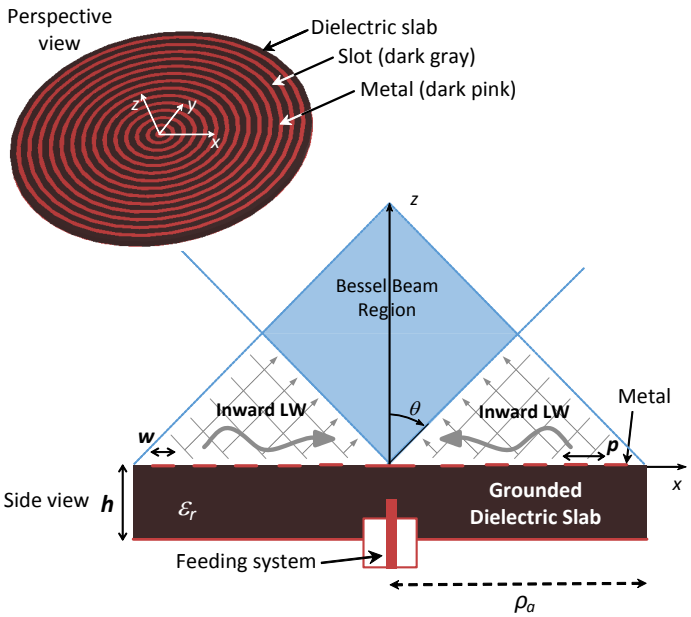

Fig. 1. Top and cross-sectional views of the considered planar antenna made by a metal strip grating (MSG) on a GDS. The diamond-shaped region (in light blue) indicates the spatial region close to the z-axis where a focused Bessel beam is created [18]. The inward cylindrical LWs, which generate this Bessel beam within the NDR, are also shown on the aperture.

Let us consider a finite circular radiating aperture of radius ρ_a orthogonal to the z-axis of the system with its origin ($\rho = 0$) at the aperture center (see also Fig. 1). In order to generate a zeroth-order beam, one would need to excite a tangential electric field over an infinite aperture placed at $z = 0$ given by (2) (being in this case $E_\phi = 0$). As originally demonstrated in [1], the truncation of this aperture with a finite radius ρ_a, required for physical realization, will limit the range where the beam is focused. In particular, an NDR can be defined, from $z = 0$ up to $z_\mathrm{NDR} = \rho_\mathrm{a} \cot\left[\sin^{-1}(k_\rho/k_0)\right]$ (see, e.g., [18]), where the field is collimated and the transverse profile can be described quite accurately by a zeroth-order Bessel function.

As analytically demonstrated in [18] for a zeroth-order beam and numerically verified in [21] for a first-order one, an inward cylindrical wave can be exploited in place of the standing-wave distribution to focus the Bessel beam inside the NDR of the launcher and around the axis of symmetry. On this basis, referring to azimuthally symmetric beams (namely, $n = 0$), the inward cylindrical wave $H_0^{(1)\prime}(\cdot)$ (first-order derivative of the Hankel function of the first kind) can replace the standing wave J_0' in (2) evaluated at $z = 0$; hence we can write

$$E_\rho(\rho, z = 0) = -j\frac{k_z}{k_\rho} E_0 H_0^{(1)'}(k_\rho \rho). \tag{4}$$

In order to synthesize such an aperture field, we propose here a novel design based on the excitation of an azimuthally symmetric cylindrical TM LW supported by an annular MSG [29]. This is achieved by means of an azimuthally symmetric source [38], namely a coaxial probe source coming through the ground plane and placed along the z-axis, i.e., at the center of the annular open waveguide and MSG.

By local linearization of the radially periodic structure in Fig. 1, the wave can effectively be seen to propagate along a one-dimensional (1-D) periodic MSG [31], [32] and thus can be described in terms of space harmonics (Floquet waves) which have some frequency dependence [39]. Assuming a direction of propagation within the unit cell along the x-axis for the linearized 1-D structure, (see Fig. 1) as completed in previous works [31], [32], the m-th Floquet space harmonic has a dispersive wavenumber defined by $k_{xm} = k_{x0} + 2\pi m/p$ where p is the radial period and $k_{x0} = \beta_0 - j\alpha$ is the wavenumber of the fundamental harmonic [29]. Typically, the structure is designed to radiate through the $m = -1$ harmonic. Thanks to this local linearization within the unit cell, one can assume that $k_{\rho m} = k_{xm}$, which is the transverse wavenumber of the cylindrical wave associated with the m-th space harmonic. This is because the radially cylindrical surface wave, propagating from the feeding point, is always perpendicular to the MSG. As a consequence, the analysis of the 1-D linearized structure can be effectively extended to the 2-D azimuthally invariant structure.

Throughout the paper we will always deal with physical LWs ($\alpha_\rho > 0$), and thus attenuating as they move radially away from the origin to generate the Bessel beams within the NDR. When considering the linearized and equivalent 1-D structure, each space harmonic has a longitudinal complex wavenumber $k_{zm} = \beta_{zm} - j\alpha_z$, related to the transverse wavenumber k_{xm} by means of the separation condition, with $\alpha_z > 0$ (*proper* harmonic) or $\alpha_z < 0$ (*improper* harmonic) according to its *backward* or *forward* nature [29], respectively.

We will select the GDS and the MSG such that the antenna operates in a frequency range where a fast space harmonic exists (e.g., the $m = -1$) and is backward, i.e., a proper LW with $\beta_{-1} < 0$. Hence, the space harmonic will propagate as an attenuated outward cylindrical wave with E_ρ proportional to $H_0^{(2)\prime}(k_{\rho,-1}\rho)$, where $k_{\rho,-1} = \beta_{-1} - j\alpha_\rho$, with $\beta_{-1} < 0$ and $\alpha_\rho > 0$. Since, in general, the relation $H_0^{(2)}(\xi) = -H_0^{(1)}(-\xi)$ holds between the zeroth-order Hankel function of the first and second kind [40], exploiting the $m = -1$ backward spatial harmonic one can recover the desired inward aperture distribution in (4) as follows

$$H_0^{(2)}(k_{\rho,-1}^{\mathrm{LW}}\rho) = -H_0^{(1)}(-k_{\rho,-1}^{\mathrm{LW}}\rho)\,, \tag{5}$$

where the superscript LW is inserted to recall that the aperture field is supported by a LW mode. This relation can be straightforwardly generalized to a nth-order aperture field [40], establishing again the desired inward character for the fields on the antenna aperture. This allows for supporting an arbitrary nth-order backward traveling-wave aperture field by means of the same MSG and the relevant fast Floquet spatial harmonic, which has to be excited by properly designing the feed system.

III. Antenna Design

To implement the 2-D periodic LWA supporting the inward traveling-wave distribution we conveniently exploit LW theory. The design of the radial structure in Fig. 1 is based on the modal analysis of an equivalent 1-D linearized lossless structure, as previously done for similar annular configurations (see, e.g., [31], [32]). To perform the modal analysis we

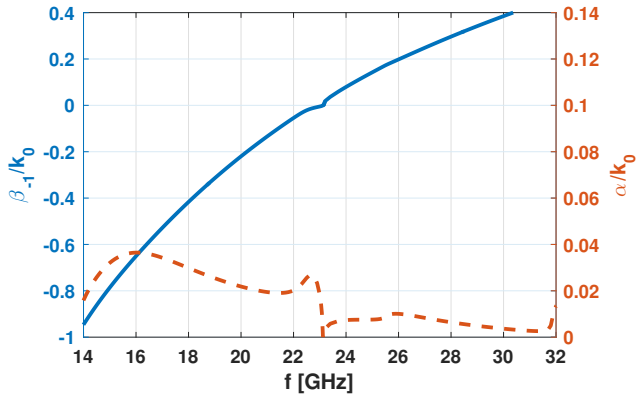

Fig. 2. MoM dispersion behavior for the normalized phase and attenuation constants for the designed LWA structure. The $m = -1$ radiating space harmonic is first in its backward (nondiffracting) regime (from 14 GHz to 23 GHz) and then in its forward (diffracting) regime (from 23 GHz to 32 GHz). Parameters of the selected structure: strip width $w = 4$ mm and period $p = 10$ mm. The supporting GDS is made by a commercial laminate with $\varepsilon_r = 2.2$ and thickness $h = 3.14$ cm.

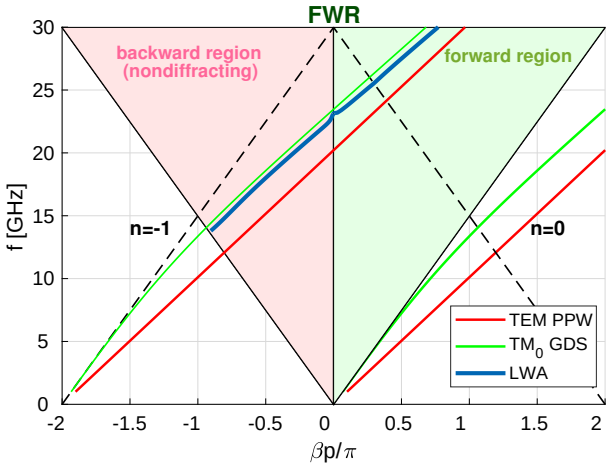

Fig. 3. Brillouin diagram for the designed LWA considering TM waves (open structure, parameters as in Fig. 2). The red curve corresponds to the fundamental (unperturbed) TEM mode of the relevant PPW (closed structure), whereas the green curve corresponds to the TM_0 mode for the GDS. The blue curve is the $m = -1$ space harmonic for the TM mode (perturbed) of the selected LWA. In addition, the triangle regions are shown defining both the bound and radiating fast-wave regions (FWRs): the light pink color highlights the backward spectral region where the wave is nondiffracting, whilst the light green color highlights the forward region where the wave is diffracting.

consider an infinite linearized structure with propagation along the x-direction (see Fig. 1), by using a MoM code developed and presented in [41] for the analysis of a single-layer phased array of microstrip LWAs [39], and recently modified in [32], to account also for dual-layer grounded substrates [42].

A. Dispersion Analysis

It should be mentioned that a preliminary analysis of the capabilities of the bull-eye printed LWA for Bessel beam generation has been assessed in [37] using the antenna structure employed in [31] (with GDS having $\varepsilon_r = 10.2$ and thickness $h = 1.27$ mm), but with an ideal source; i.e., a vertical electric dipole. Unfortunately, it was found in [37], that, when exciting this structure with a 50-Ω coaxial probe a very narrowband behavior (about 4% fractional bandwidth around 18 GHz) was obtained. This was mainly due to the high value of the permittivity of the dielectric substrate along with the slab thickness and broadband mismatches.

In the following we propose and develop a completely new and optimized antenna design, as depicted in Fig. 1, based on a commercial laminate having permittivity $\varepsilon_r = 2.2$ and thickness $h = 3.14$ mm, which can produce a considerably wider operational bandwidth; i.e., from 14 GHz to more than 21 GHz, resulting in a fractional bandwidth equal to more than 40%. Given these design considerations, the antenna operates in a unimodal regime. Also, the adopted MoM dispersive analysis for the radially periodic LWA, as done for similar far-field designs (see, e.g., [31], [32]), corresponds to a 1-D linearized version of the radial structure. This modeling approach will also be validated and corroborated in the next sections by means of a theoretical Bessel beam analysis, LW theory, full-wave simulations, and experimental validation. By considering the supporting GDS, a MSG can be designed and placed on top to transform the surface wave supported by the GDS to a LW mode. The perturbation produced by the MSG should be large enough to generate appreciable values of the leakage constant (typically α/k_0 of the order of 10^{-2}). To operate in the desired range of frequencies centered around 18 GHz with the selected commercial laminate, a dispersive analysis on the two limit-case background guiding structures having thickness h (i.e., the GDS and the parallel-plate waveguide (PPW)) has allowed us to fix the period p of the MSG to 10 mm.

To design the width of the strip we have completed a parametric analysis for different values of w: increasing the values of w produces stronger perturbation and larger values for the attenuation constant, whilst the phase constant remains substantially unperturbed being its behavior mainly determined by the period p. Since the leakage rate also determines the size of the aperture needed to radiate a fixed amount of the input power and to deal with a practically-sized LWA, we consider here a value of w equal to 4 mm, which corresponds to $\alpha/k_0 = 0.03$ at $f = 18$ GHz. The normalized dispersion curves β_{-1}/k_0 and α/k_0, in both the forward and backward regimes are shown in Fig. 2. It can be observed that the normalized phase constant for the considered spatial harmonic increases regularly with frequency passing through broadside, i.e., $\beta_{-1}/k_0 = 0$, at a frequency value f_c equal to about 23 GHz (corresponding to the presence of an open stop-band [29], [31], [32], for which $\beta = 0$). This defines a *proper* LW, $\Im\{k_{z,-1}\} < 0$, with a pointing angle θ_p for the conical far-field pattern that will scan from backward endfire to broadside (for frequencies lower than f_c), and an *improper* LW, $\Im\{k_{z,-1}\} > 0$, from broadside to forward endfire (for frequencies higher than f_c) [29], [31].

When considering the near-field region of the antenna, the *proper* LW will define an inward traveling wave which instead, as theoretically discussed in the previous section and verified next, is able to generate a nondiffracting Bessel beam. We should mention that the attenuation constant in Fig. 2 shows an abrupt change of the leakage rate with a null point at the

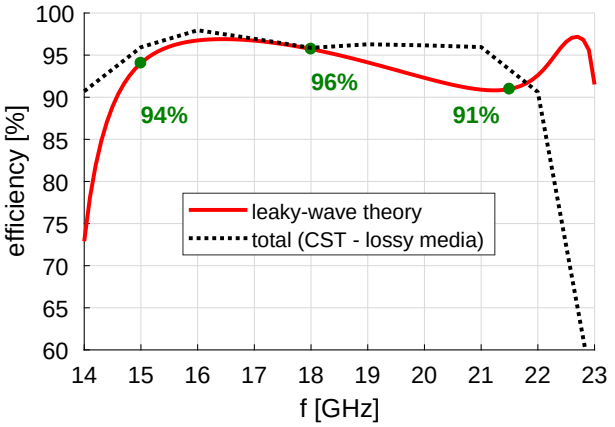

Fig. 4. Efficiency versus frequency for the designed LWA.

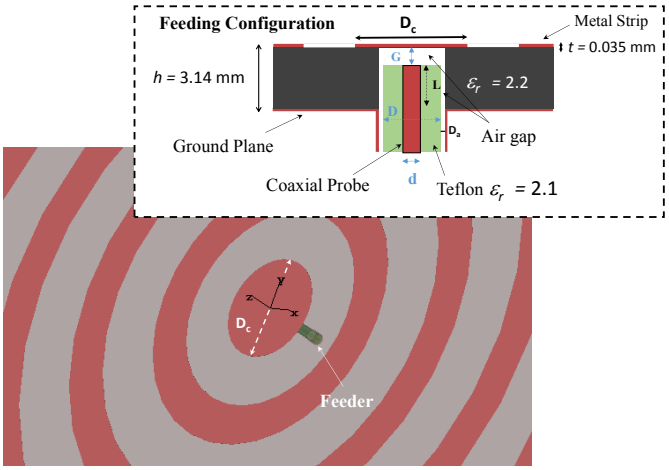

Fig. 5. Feeding system for the designed LWA (dielectric slab in transparency). The main geometric parameters are illustrated in the figure inset: $D = 0.99$ mm, $d = 0.31$ mm, air gap $G = 0.44$ mm, $L = 2.7$ mm. The diameter of the circular disk at the origin is D_c (= 10 mm) and the thickness of the top MSG and bottom ground plane is $t = 0.035$ mm. The parameter D_a models a very small vertical air gap around the coaxial probe and teflon dielectric coating that can occur during LWA fabrication and probe connectivity.

broadside frequency, which is the typical effect of the open stopband in this class of structure (see, e.g. [31], [32], and refs. therein). However, the permittivity of the GDS, the period and width of the MSG have been suitably selected to obtain sustained leakage in the backward quadrant, since the antenna has been designed to radiate a Bessel beam by means of the fast backward spatial harmonic.

The corresponding Brillouin diagrams, obtained by considering that $\beta_{x-1} = \beta_{x0} - 2\pi/p$, for both the unperturbed and perturbed TM modes, are presented in Fig. 3. In particular, the perturbed fundamental TM spatial Floquet harmonic ($m = -1$) of the MSG, and the phase constants of the two related unperturbed spatial harmonics supported by the insightful limit-case structures (i.e., the TM_0 of the open GDS and the TEM of the closed PPW, respectively) for the considered LWA, are also shown in Fig. 3. As expected, the phase constant for the fast spatial harmonic is closer to the green curve representing the unperturbed TM_0 mode of the GDS, since the ratio $w/p < 1/2$ and hence the unmetalized area of the air-dielectric interface within the unit cell is larger than the metalized one.

In the diagram the backward and forward regions are highlighted with two different colors, defining the relevant nondiffracting and diffracting regions for the LWA. Interestingly, the presence of the open stopband region [29] (occurring at about $f_c = 23$ GHz), where the radiative performance of the LWA deteriorates being theoretically $\beta_{-1} = 0$ and $\alpha_\rho = 0$, represents the frequency transition point from a collimated (or nondiffracting) to a diverging (or diffracting) near-field distribution. Furthermore, one can expect that when f is close to f_c the antenna loses its capabilities to collimate the field since the required backward traveling LW mode is no longer supported on the aperture, and the antenna total efficiency quickly reaches very small values. For example, in Fig. 4 the total antenna efficiency from CST reduces below 60% at 23 GHz ($= f_c$).

The theoretical antenna efficiency within the considered frequency range, evaluated with the standard formula based on LW theory [29, Ch. 7, Eq. 7.28], is also reported in Fig. 4. As expected, the behavior of the red curve in Fig. 4 reflects the trend of the attenuation constant of the leaky mode supported by the structure (see Fig. 2), but it is not able to account for both ohmic and dielectric losses. However, the total antenna efficiency (lossy media) in Fig. 4 using CST accounts for these losses as well as the metal thickness, as shown in Fig. 5.

We should mention that this total efficiency curve from full-wave simulations is always slightly greater than the one obtained by LW theory below the open stopband region. This is likely due to the fact that the theoretical efficiency does not account for the presence of spurious radiation (such as, e.g., the one occurring due to surface waves at the antenna truncation), which actually occurs over all of the considered frequency range, and are not taken into account by the LW model. As a matter of fact, the theoretical model assumes that the residual power is perfectly absorbed at the aperture truncation and that limited radiation occurs, in the form of LWs, close the open stopband and close to the lower bound region of the fast-wave region [29]. In addition, the theoretical efficiency curve given by the LW attenuation constant for the linearized 1-D unit cell by MoM does not account for any feed mismatches near the open stopband which are actually taken into consideration in the full-wave CST simulation model.

B. Details on the Practical Feeding System

A key feature of LWAs is their planar and low-cost profile as well as the simple feeding system required to excite the wave inside the open waveguide, in contrast with much more complicated feeding networks needed, e.g., by array configurations [12] and for generation of Bessel beams in the optical region [5]. We use here a vertical 50-Ω coaxial probe feeding arrangement, similar to the one designed in [19] and [27]. In our work, the feed system is able to effectively launch an outward cylindrical wave that is turned into a CLW with a backward $m = -1$ spatial harmonic by the top MSG.

As shown in Fig. 5, we have modeled in CST a 50-Ω coaxial cable connector that penetrates the cavity through the

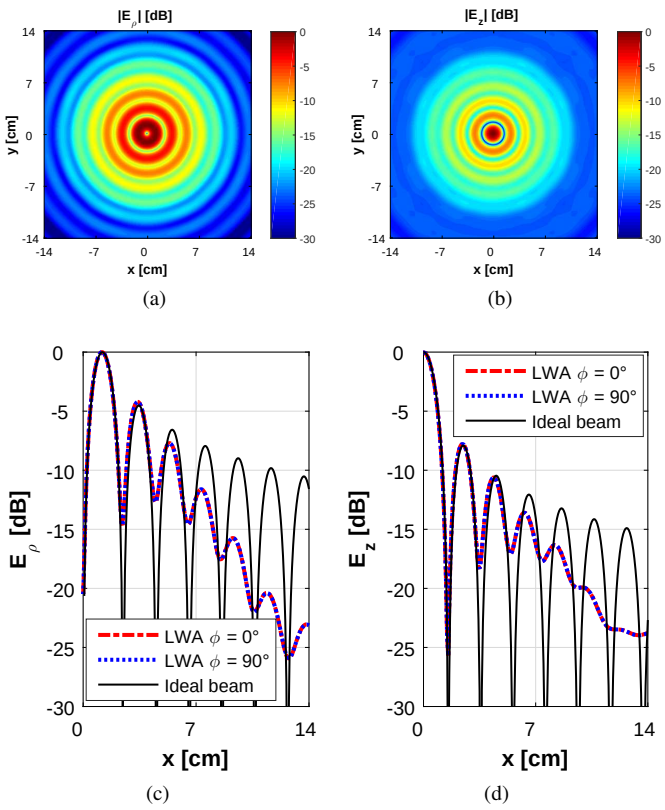

Fig. 6. Near-field at $f = 18$ GHz obtained by simulating the finite LWA described in Fig. 1 using CST with the implemented feeding system as in Fig. 5. Results are also compared to a theoretical Bessel beam (generated on an ideal and infinite structure) where a general agreement with the position of the field maxima and the pattern nulls can be observed. Field maps for (a): E_ρ and (b): E_z on a transverse plane z_0 ($= z_{\rm NDR}/2 = 15.5$ cm) with the 1-D profile of these components in the same horizontal plane for (c): E_ρ and (d): E_z. Note: The colormap legend in (a) and (b) and the relevant dynamic range are assumed as reference cases for the field maps presented in the following.

ground plane. To accommodate the internal probe along with the dielectric insulator, a hole having diameter about 1 mm was drilled in the GDS. Both the probe penetration inside the cavity and the diameter D_c of the first disk of the top MSG (see Fig. 5) have been tuned by means of a parametric analysis to optimize for 50-Ω input matching. All the involved parameters along with a detailed configuration of the feeding system are illustrated in Fig. 5 and inside the relevant caption.

IV. Numerical Results

In this section, we examine the near-field radiated by the LWA designed in Section III to validate the proposed structure, which supports an $m = -1$ fast spatial harmonic over an aperture having radius ρ_a. We demonstrate the capability of this design to generate a Bessel beam over a significantly wide frequency band, starting from the initial design frequency $f = 18$ GHz, where $k_{\rho,-1}^{\rm LW} = (-0.42 - j0.03)k_0$. To deal with a practically sized antenna and to maximize the efficiency obtaining a value greater than 90% at $f = 18$ GHz, we have selected a radius $\rho_a = 14$ cm. This determines a total of 14 unit cells along the radial direction.

Near-field distributions radiated by the prototype on both the parallel and normal planes, with respect to the antenna aperture, will be presented next. To this aim, full-wave simulations using CST, exciting the antenna with the realistic feeder presented in Fig. 5, are developed to account for the metallic thickness t. To avoid the simulation of a large domain, the near-field is evaluated by exporting the aperture distribution and calculating the relevant radiation integrals involving the equivalent sources [43]. The result is compared with that of an ideal beam, namely the one generated by an ideal infinite structure, which supports the field distribution in Eq. (2) for $z = 0$ and $n = 0$.

The normalized transverse and longitudinal components, E_ρ and E_z (in dB), on the xy plane (i.e., parallel to the antenna aperture) at a distance equal to half the NDR calculated at the design frequency $f = 18$ GHz (where $z_{\rm NDR} = \rho_a \cot\left[\sin^{-1}\left(|\beta_{\rho,-1}|/k_0\right)\right] = 31$ cm) are reported in Figs. 6(a) and (b), whereas the 1-D profile of the two components on the same plane but depicted along the two principal planes (i.e., the xz-plane ($\phi = 0°$) and the yz-plane ($\phi = 90°$)) are presented in Figs. 6(c) and (d).

A good agreement is observed between the radiated leaky aperture field from CST and the ideal Bessel beam close to the z-axis as shown in Figs. 6(c) and (d). For example, the position and amplitude for the field maxima (in dB) and the pattern nulls are consistent. These results are expected and follow the earlier demonstration in [18] for nondiffracting Bessel beams. Thus our results in Fig. 6 suggest that the field radiated by the inward LW on the antenna aperture agrees very well with the J_0' Bessel function (describing the ρ-component of the field) and with J_0 (describing, instead, the z-component), as in (2) and (1), respectively, with $n = 0$. It should also be mentioned that a discrepancy between the simulated LW field and the ideal Bessel beam (amplitude only) can be observed for increasing values of x. This is because, as identified in [18], the excited inward field on the aperture approximates the Bessel beam very well close to the vertical axis, whilst the agreement gradually deteriorates away from the axis [18]. Also, the beams present an azimuthally invariant behavior (not visible here), provided by the geometric symmetry of the structure as well as by the feeding system.

In Figs. 7(a)-(h) the radial component of the electric field distribution over the xz-plane, up to the NDR (namely, $z_{\rm NDR} = 31$ cm at $f = 18$ GHz) is reported. The field maps are shown over a wide frequency band, from 15 GHz (reported in Fig. 7(a)) up to 21 GHz (reported in Fig. 7(h), see figure headers for the relevant values). The field maps in Figs. 8(a)-(h) report the vertical component of the electric field over the same frequency range. It is seen that the electric field remains well collimated up to the NDR, which depends on the operational frequency and the aperture radius. However, we have observed that starting at about 20 GHz the E_z component degrades more quickly with respect to the transverse component E_ρ. As discussed in [18], the inward aperture field defines a conical region having angle $\theta_a = \sin^{-1}(\beta_\rho^{\rm LW}/k_0)$, which coincides here with the shadow boundary defined by the LW traveling on the aperture [29].

As expected, the higher frequency, namely $f = 21$ GHz, provides the largest NDR. For comparison, the plot in Figs. 7 and 8 are always shown up to $z_{\rm NDR} = 31$ cm; we have

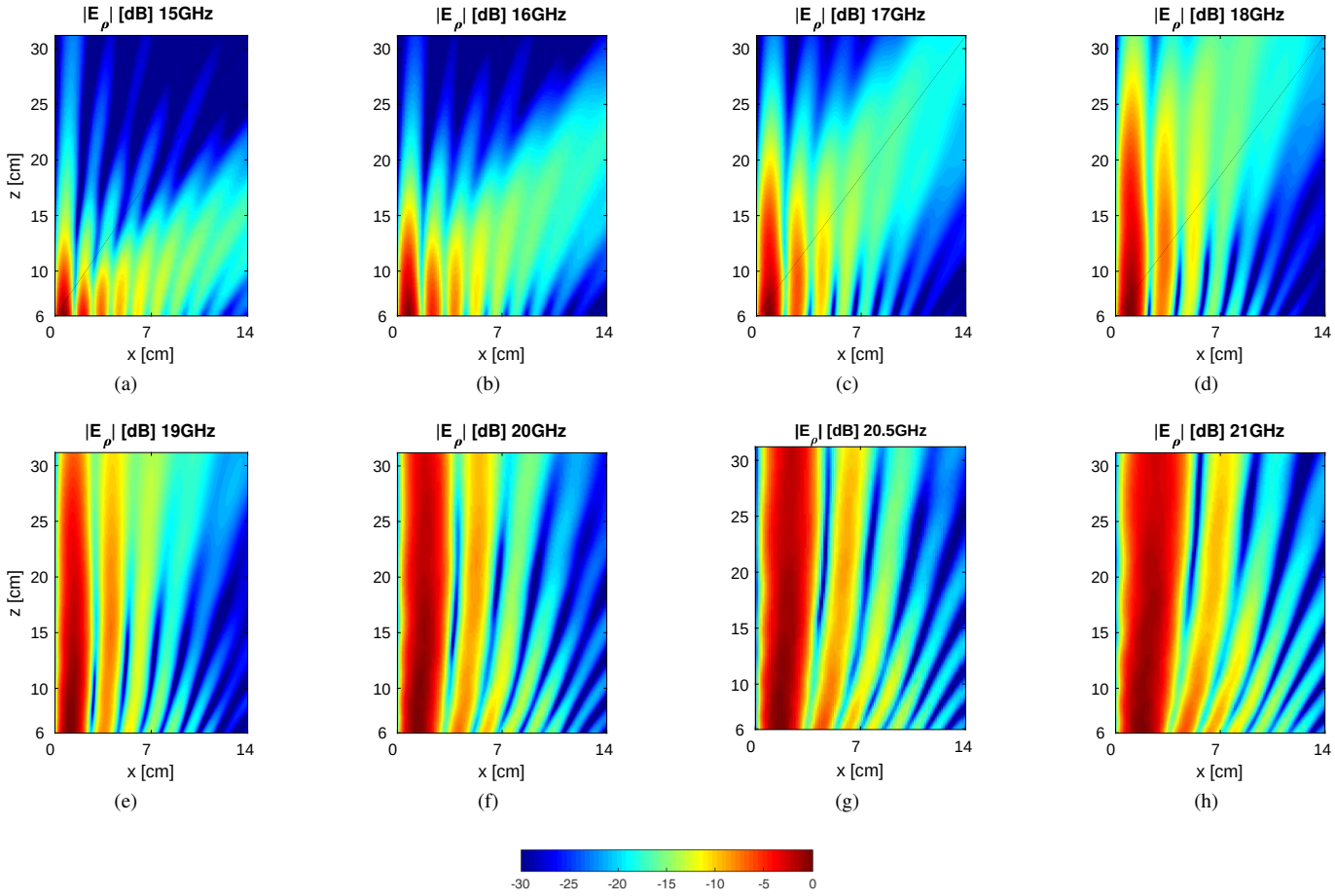

Fig. 7. Simulated distribution of the electric field radiated in the near-field on the xz-plane (i.e., $\phi = 0°$) by the designed LWA using CST, up to the NDR for the antenna calculated at the design frequency $f = 18$ GHz: (a)-(h) ρ-component for frequencies going from 15 GHz to 21 GHz.

verified that, at 21 GHz, the beam remains collimated up to the range predicted by the theory, namely $z_{\mathrm{NDR}} = 103$ cm (corresponding to $\beta_\rho^{LW} = 0.13k_0$). Depending on the application, one can flexibly use the entire bandwidth made available by this type of LWA (in our design, from about 15 GHz to about 21 GHz), which is able to generate a focused distribution having a variable NDR and beam size.

We finally stress that our proposed wideband LWA design gives the desired flexibility in the choice of the operational frequency range and of the relevant transverse wavenumber k_ρ^{LW}. This is in contrast with previous designs based on holographic principles where the phase constant should be fixed *a priori* to synthesize the aperture field required to generate the desired Bessel beam [18]-[21].

V. Experimental Validation

The antenna prototype designed and optimized in the previous sections was measured in a calibrated anechoic chamber. A picture of the realized structure is reported in Fig. 9, which shows the top and bottom side of the manufactured bull-eye antenna, fed by means of the 50Ω connector and the coaxial transition as described in Sec. III and Fig. 5, manufactured by the SRI Connector Gage (part number 85-131-1000-80). The antenna is made on a Taconic TLY5 substrate with permittivity $\varepsilon_r = 2.2$ and thickness $h = 3.14$ mm.

The simulated and measured reflection coefficient is reported in Fig. 10, where we also show the comparison with the simulated input matching of the antenna design proposed in [37] supported by the GDS employed in [31] (defined by $\varepsilon_r = 10.2$ and a thickness of 1.25 mm), and driven by a similar 50-Ω coaxial probe coming from the bottom ground plane. As clearly visible, the structure proposed in [37] is poorly matched around 18 GHz. This is not surprising since the LWAs designed in [31] were optimized to work with a planar surface-wave launcher feed system and GDS having $\varepsilon_r = 10.2$. Also, this feed system did not offer the required full azimuthal symmetry, thus the LWAs in [31] were not suitable to launch a Bessel beam.

Regardless of these facts, our proposed antenna for Bessel beam generation is very well matched around the main design frequency (i.e., $f = 18$ GHz) and inside a very wide operational frequency band, from 14 GHz to 21 GHz as shown in Fig. 10, resulting in a fractional bandwidth equal to about 40%. We note that the measured input reflection coefficient is almost never superimposed with the simulated one, even though it is well below the conventional threshold metric of -10 dB inside the considered frequency range. The observed

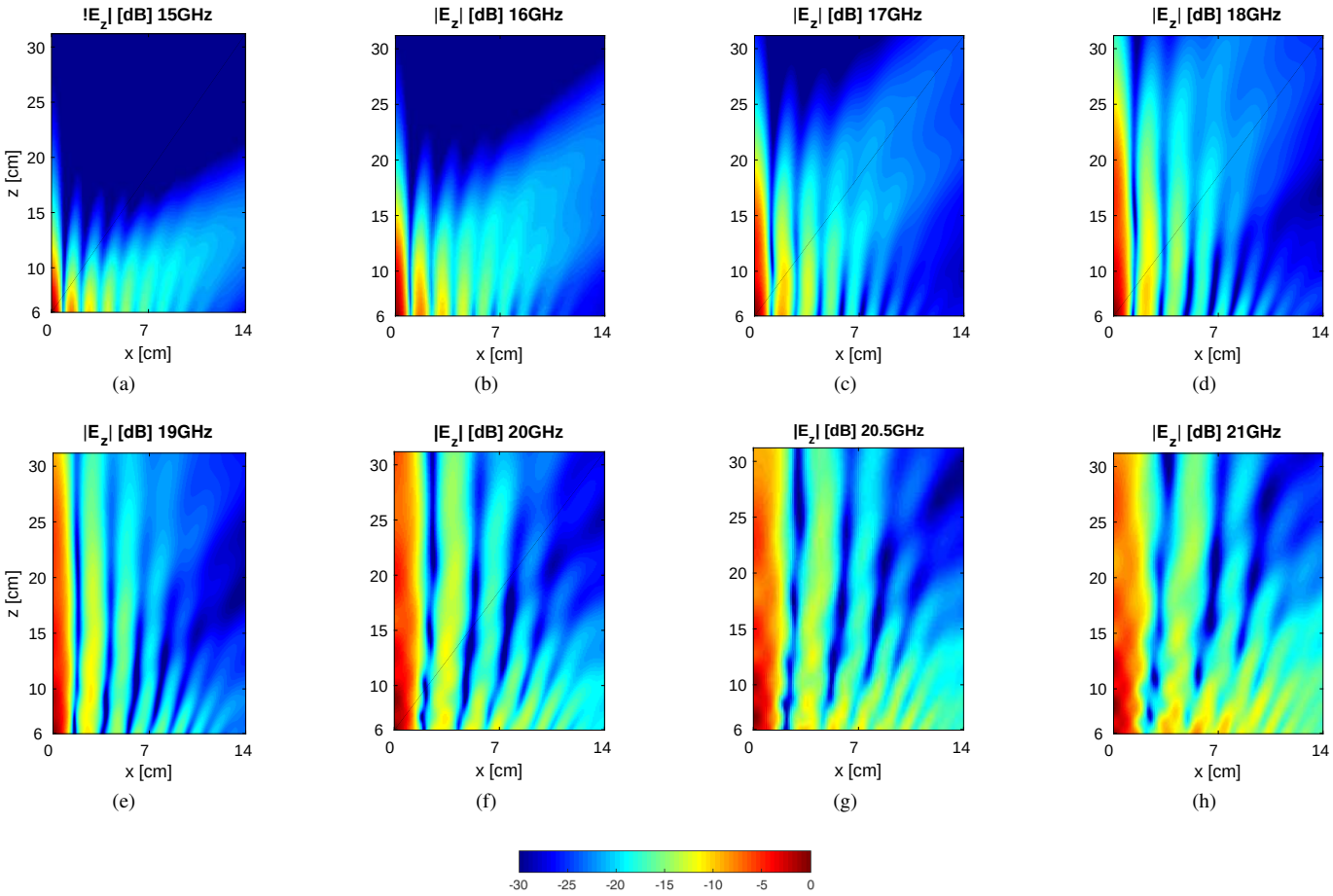

Fig. 8. Same as in Fig. 7 but for the z-component of the field.

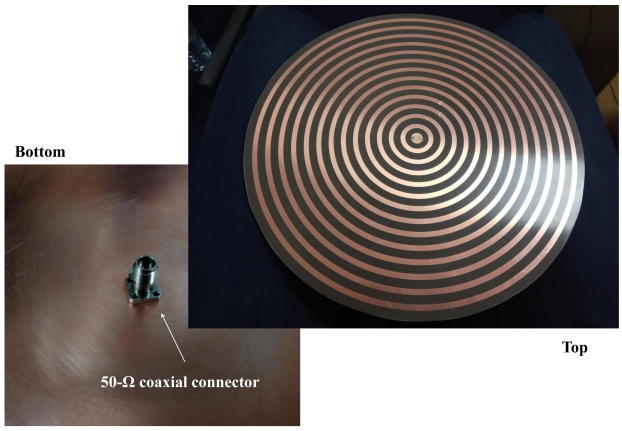

Fig. 9. Picture of the fabricated bull-eye antenna. The copper color is the annular metallic strip arrangement.

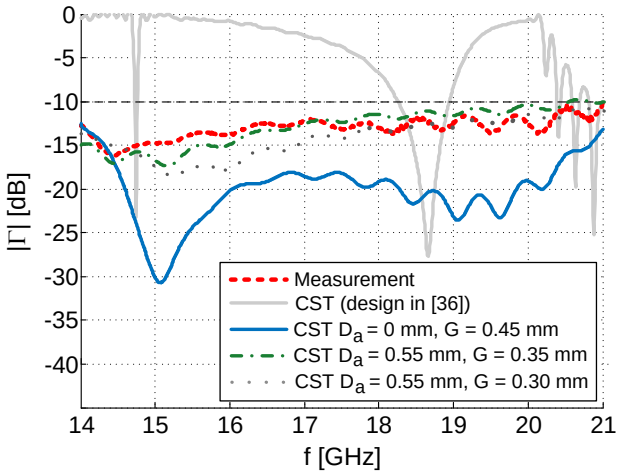

Fig. 10. Measured and simulated reflection coefficient (absolute value in dB) at the input for the manufactured LWA prototype. The horizontal dashed black line indicates the conventional threshold for $|\Gamma| \leq -10$ dB. Results are also compared to simulations of our preliminary structure presented earlier in [37] and of a structure with a small error for the dimension G (see Fig. 5) and a very small vertical air gap which may have occurred during fabrication defined by D_a. For the optimized structure $G = 0.45$ mm and $D_a = 0$ mm.

minor discrepancy between the measurements and simulations is likley due to the fabrication tolerances, mainly related to the difficulties in accurately controlling the air gap G, as depicted in Fig. 5, as well as the drill hole diameter in the GDS to accomodate the coaxial transition.

To further investigate these fabrication tolerances, a parametric analysis was completed in CST by varying G and

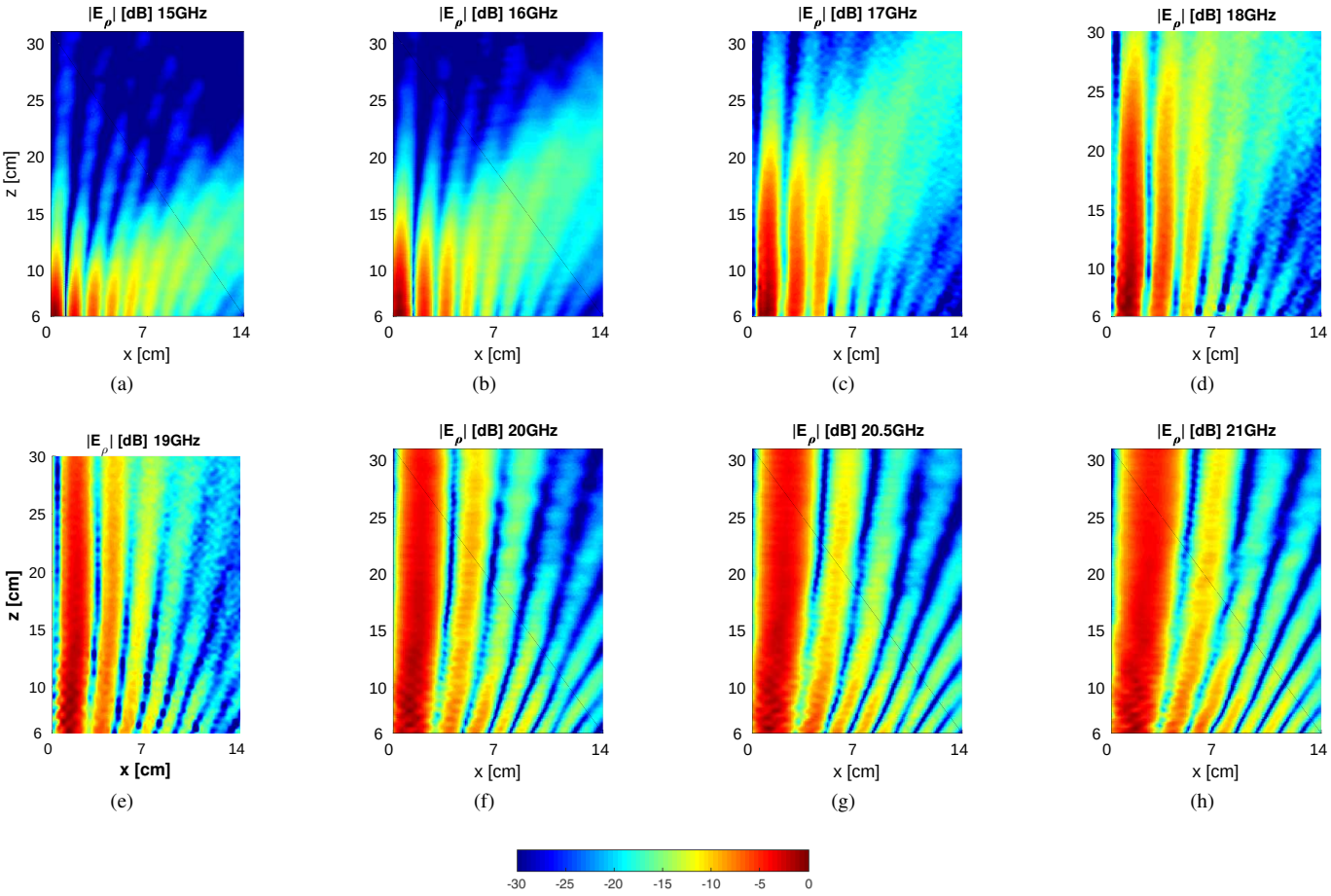

Fig. 11. Measured longitudinal 2-D profile of the electric field radiated in the near-field in the xz-plane (i.e., $\phi = 0$) up to $z_{\rm NDR}$ = 31 cm. (a)-(h) ρ-component for a frequency going from 15 GHz to 21 GHz at a step of 1 GHz.

D_a, which describe these two critical parameters: mainly, the height of the air gap G and the undesired vertical air gap surrounding the coaxial probe and teflon dielectric defined by D_a (see Fig. 5). As observed in Fig. 10, a very good agreement can be obtained between the full-wave simulation results and the measurements by accounting for the presence of these small errors on G and D_a that occurred during the PCB drilling process and assembly of the coaxial transition with the LWA.

To measure both the longitudinal and transverse components of the radiated near-field, the probe used for the measurements has been deployed in different orientations, and automatically translated on the selected xy plane by means of a mechanical controller. An absorber is placed around the probe to minimize the reflections occurring between the probe metalization and the antenna aperture, which are expected to produce smaller oscillations in the field profile, gradually attenuated moving farther from the antenna toward the NDR. It is noted that the measured data, sampled at spatial steps equal to 3 mm over the xy plane, are raw, and that no post-processing, filtering or smoothing algorithms have been applied.

The normalized transverse component of the electric field along the xz plane is reported in Figs. 11(a)-(h), moving the probe from close to the antenna aperture (6 cm) up to a distance $z_0 = 31$ cm; six different frequencies are considered, reported in Figs. 11(a)-(h), respectively (see the figures' headers for the relevant details). Figs. 12(a)-(h) show the z-component of the electric field over the same 2-D area and for the same frequency values. These experimental results are in excellent agreement with the simulated 2-D distributions presented in Figs. 7 and 8. It is clearly visible that the inward LW field distribution on the aperture is able to generate a Bessel beam along the longitudinal plane and within the NDR. Also, the field remains collimated up to larger distances for increasing values of frequency. The null point along the z-axis for the transverse component of the field is also well defined.

To better understand the longitudinal profile of the two field components, in Figs. 13(a) and (b) we report a comparison between measured and simulated results along z for the three measured frequencies. In particular, Fig. 13(a) presents the comparison for the ρ-component along the axis parallel to the z-axis containing the first maximum of the ideal Bessel beam component, which coincides with the first maximum of the Bessel function J_1. Similarly, Fig. 13(b) gives the results for the z-component along the z axis. Overall, a very good agreement has been obtained, especially for increasing values of z. Some oscillations are visible closer to the antenna aperture, which gradually reduce for increasing distances.

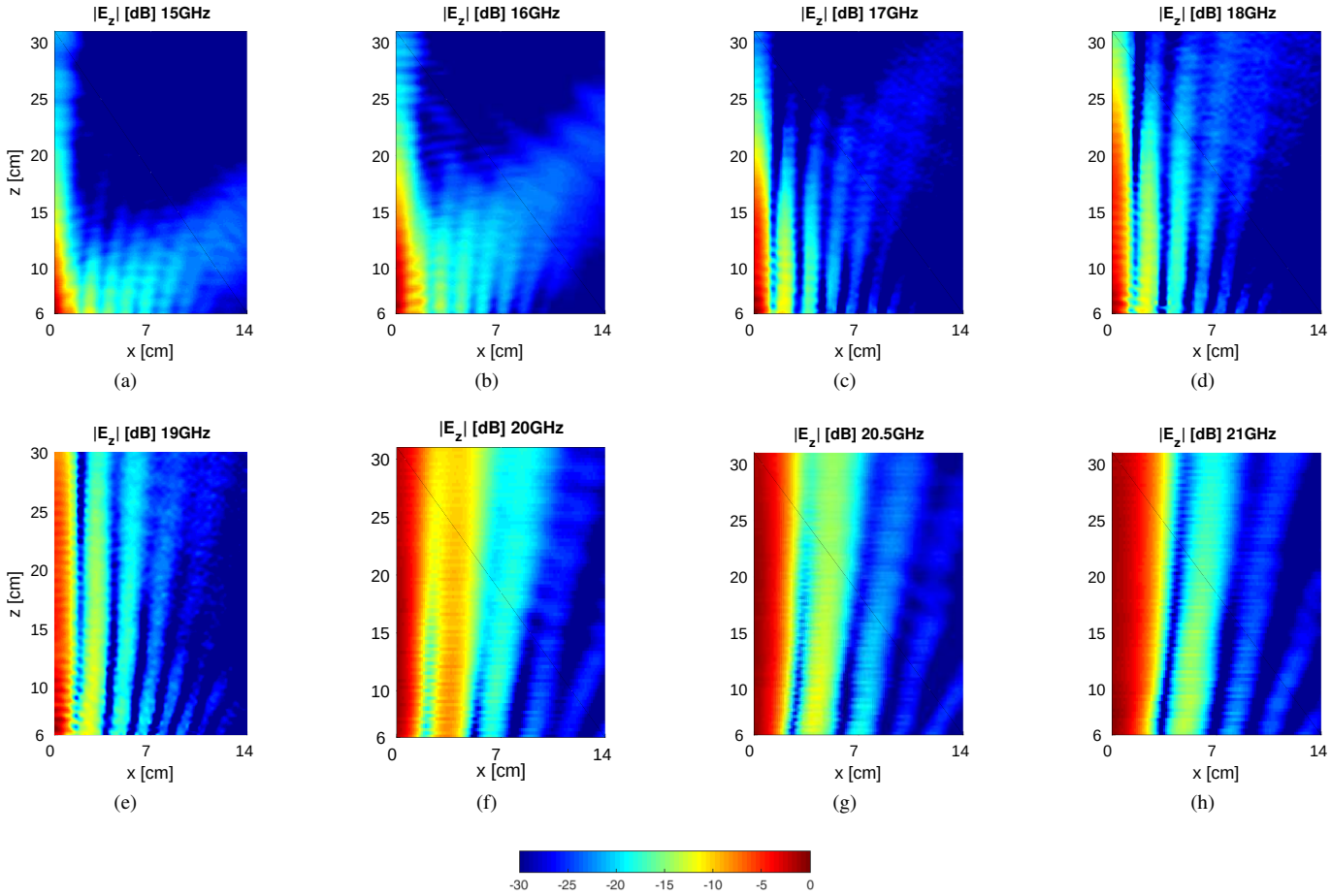

Fig. 12. Same as in Fig. 11 but for the z-component of the field.

It is noted that, due to the presence of a complex longitudinal wavenumber characterizing the inward aperture distribution, and of the relevant attenuation constant α_z, the field along z in Fig. 13 decreases almost monotonically. This is in contrast with the behaviors reported with the RLSA design in [19] and the radial waveguide in [20], where the field shows strong oscillations inside the main near-field beam for the z-component of the field.

Figs. 14(a)-(c) report a comparison along z of the ratio $|E_\rho|/|E_z|$ between measured and simulated results, for the three measured frequencies as in Fig. 13. This allows us for assessing and highlighting the stronger contribution to the total field provided by the ρ-component of the field, which is also less attenuated moving away from the aperture with respect to the z-component. It is well-known that $|E_\rho|$ dominates on $|E_z|$ in the far field, whereas results in Fig. 14 extends this behavior to the near-field.

The measured component E_ρ on a transverse plane for two different values of the distance z_0 from the antenna aperture are presented in Figs. 15(a)-(f). In particular, two distances $z_0 = 15.5$ cm and $z_0 = 23.3$ cm that correspond to half of the 18-GHz NDR and $3/4$ of the NDR, respectively, are considered (Figs. 15(a) and (b) reports the operating frequency $f = 17$ GHz, Figs. 15(c) and (d) the frequency $f = 18$ GHz, and, Figs. 15(e) and (f) the frequency $f = 19$ GHz). We note in particular that Fig. 15(c), namely $z_0 = 15.5$ and $f = 18$ GHz, is in excellent agreement with the corresponding 2-D simulated map reported in Fig. 6(a). Fig. 16 reports the measured E_ρ component of the two extreme frequencies on a transverse plane for $z_0 = 5.5$ cm and $z_0 = 15.5$ cm, which represent half the NDR at 15 and 18 GHz, respectively. The relevant radial cuts are in excellent agreement with the simulated results.

To quantitatively assess the achieved agreement between the Bessel beam generated by the inward LW aperture field distribution and the ideal beam (i.e., generated by an infinite aperture, and described by the Bessel function in Eq. (1)–(3)), we finally report in Figs. 17(a)-(f) the measured 1-D cuts of the E_ρ component on the two principal planes $\phi = 0°$ and $\phi = 90°$, at $z_0 = 15.5$ cm. They are in excellent agreement with the ideal Bessel beam (i.e., with the theoretical profile given, in this case, by $J_0'(k_\beta^{\mathrm{LW}}\rho)$, assuming $k_\rho^{\mathrm{LW}} \approx \beta_\rho^{\mathrm{LW}}$). The radial cut has been reported for positive and negative values of the ρ-axis to fully assess the azimuthal symmetry of the beam. Overall, the designed LW distribution is able to accurately and efficiently generate a nondiffracting wave within the NDR of the launcher.

We should mention that the radial cuts in Fig. 17(a)-

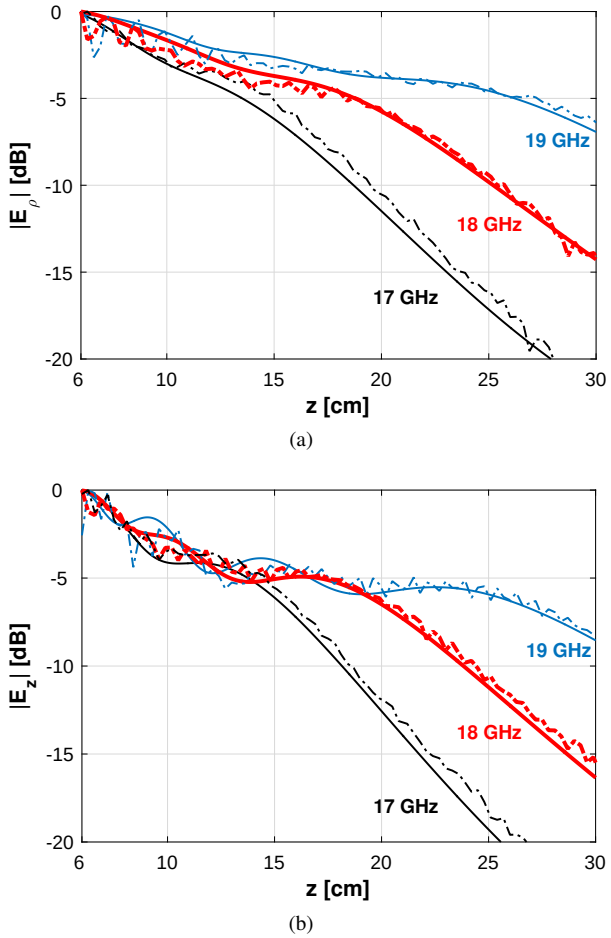

Fig. 13. Comparison of the measured and simulated 1-D longitudinal profile of the electric field (CST solid lines, measurements dashed-dotted lines). (a) $|E_\rho|$ over the first maximum along the z axis which corresponds to the first maximum of the J_0' function as in eq. (2); (b) $|E_z(\rho = 0)|$.

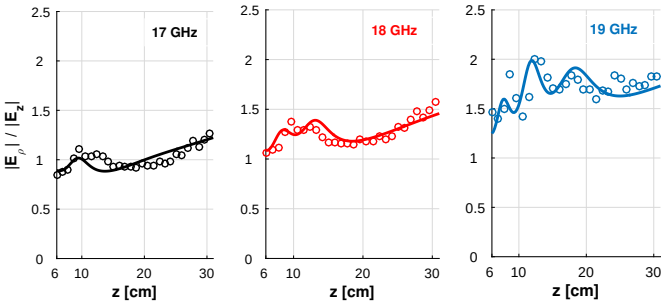

Fig. 14. Comparison of the measured and simulated 1-D longitudinal profile of the ratio between E_ρ and E_z (CST solid lines, measurements circles) for (a) 17 GHz, (b) 18 GHz and (c) 19 GHz.

(f) have been obtained by fixing z_0 to 15.5 cm (which is equal to $z_{\mathrm{NDR}}/2$ at 18 GHz). Hence, the radial profile of the beams in Figs. 17(a), (b), reporting the frequencies f = 15 GHz and 16 GHz, respectively (for which z_{NDR} = 11 cm and 16 cm, respectively), show a deteriorated agreement with respect to the theoretical profile $J_0'(k_\beta^{\mathrm{LW}}\rho)$ (that indeed would be supported by a structure having an infinite radial aperture). In particular, since the nondiffractive range increases

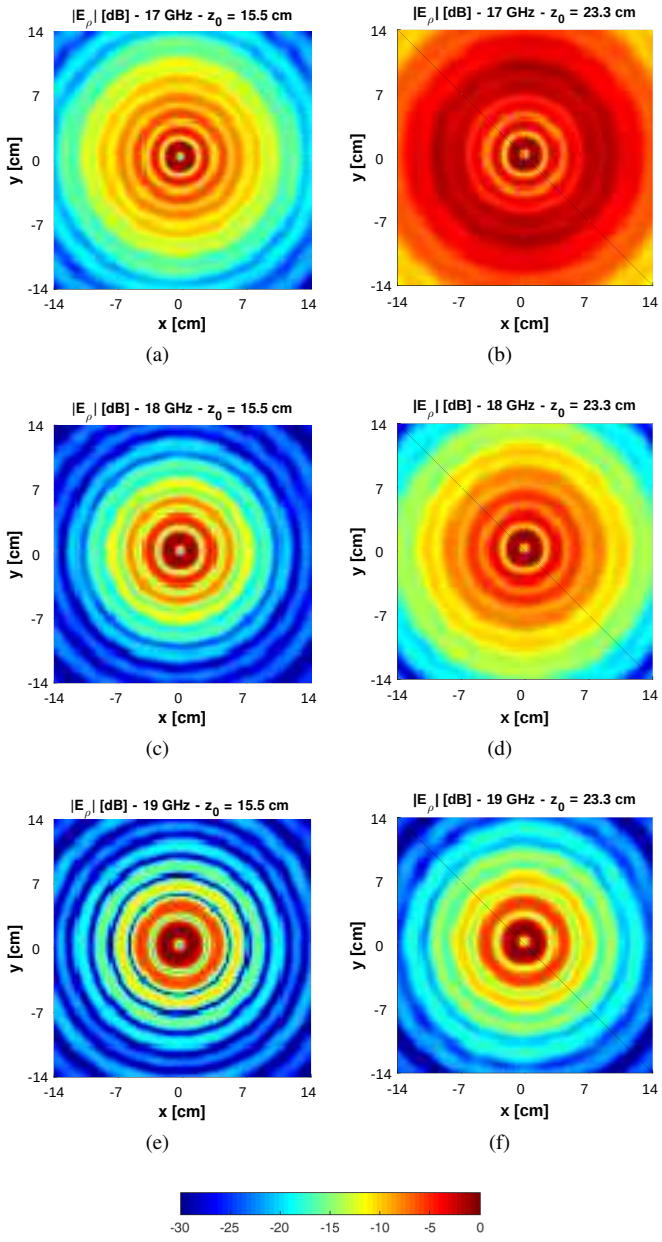

Fig. 15. Measured 2-D profile of the transverse component of the electric field in the xy-plane. (a)-(b) f = 17 GHz, z_0 = 15.6 cm and 23.3 cm; (c)-(d) f = 18 GHz, z_0 = 15.6 cm and 23.3 cm; (e)-(f) f = 19 GHz, z_0 = 15.6 cm and 23.3 cm. It should be mentioned that (b) is just beyond the NDR, where it can be observed that the field quickly starts to diffract.

with frequency, while measurements are taken at a fixed vertical distance, the agreement with the theoretical profiles is also expected to change with the frequency. This aspect has been described in Fig. 17(g) where the evolution of the nondiffractive region has been qualitatively reported. As is shown, the radial extent x_{NDR} (i.e., the dashed green line in Fig. 17(g)) of the nondiffractive region changes with frequency reaching a maximum (i.e., $\mathrm{x_{max}} = \rho_a/2$) at f = 18 GHz where measurements are taken exactly at $z_{\mathrm{NDR}}/2$, and then gradually diminishes. However, Fig. 16(a) shows the measured 2-D maps for f = 15 GHz inside the relevant NDR where the expected Bessel-beam profile can be observed and we have verified the

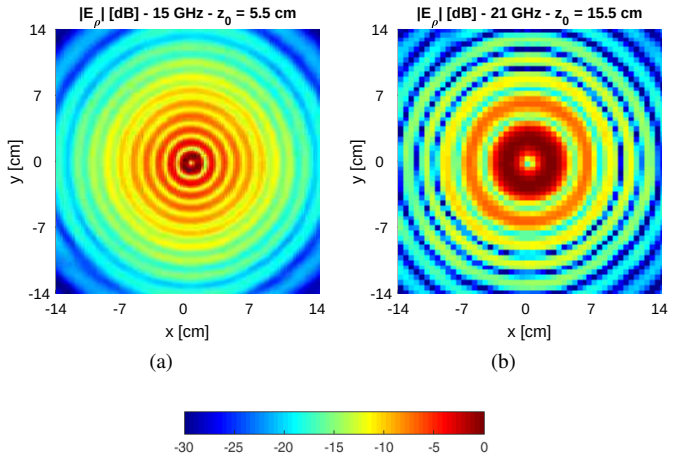

Fig. 16. As in Fig. 15 but for the two extreme frequencies: (a) $f = 15$ GHz at $z_0 = z_{\text{NDR}}/2 = 5.5$ cm, and (b) $f = 21$ GHz at $z_0 = 15.5$ cm.

agreement of the field behavior along an arbitrary radial cut with the corresponding theoretical beam profile.

To accurately assess the capabilities of the proposed design for generating a Bessel beam over a wide frequency range, Fig. 18 shows the experimental behavior of the phase constant of the leaky mode supported by the structure. The estimation has been generated on the radial cuts taken on a transverse plane at a distance equal to half the NDR for frequencies values up to 18 GHz and for a distance equal to 15.5 cm for greater frequencies (we stress that within the NDR, thanks to mentioned inward approximation, the near-field profile is accurately described by the relevant Bessel function, so that the choice of the distance has no effect on the estimation accuracy). One can simply relate either the value of the first maximum or the first null of the radiated near-field to those of the relevant theoretical Bessel function (i.e., with the radial profile given by $J_0'(k_\beta^{\text{LW}}\rho)$), whose theoretical positions are numerically known a priori. This estimation can be performed as long as the position of either the maximum or the null is within x_{NDR} (see Fig. 17(g)). For $x > x_{\text{NDR}}$ the inward approximation no longer holds, thus affecting the estimation procedure. Note that the value of x_{NDR} varies with the selected z_0. In this specific case, i.e., for $z_0 = 15.5$ cm, an accurate estimation is possible up to 21 GHz.

In Fig. 18, the results show agreement over the frequency range from 15 to 21 GHz, which validate the theoretical LW approach based on the numerical dispersion analysis of the linearized MSG structure and assess the claimed wideband capabilities. For frequencies smaller than 15 GHz the NDR is too small (smaller than 10 cm, as seen in Fig. 18, right axis). In addition, in this frequency region, i.e., the transition region, the LW aperture field gradually loses its dominant character [44]. For frequency values close to the open stopband of the antenna (occurring at about $f_c = 23$ GHz), radiation is no longer supported, as also corroborated by the total efficiencies reported in Fig. 4.

VI. Conclusion

We have presented and experimentally demonstrated the possibility of generating a Bessel beam by means of a backward spatial harmonic supported by a radially periodic two-dimensional LW antenna over a wide frequency range. The structure is able to successfully synthesize an inward traveling-wave aperture distribution over a wide frequency range, from 15 GHz to 21 GHz, and to effectively generate a Bessel beam within the nondiffracting range (up to distances larger than 1 meter with an aperture having radius $\rho_a = 14$ cm). The radiator provides the desired flexibility in the choice of the transverse wavenumber for the beam.

The proposed design may represent an attractive low-cost solution for the generation of collimated fields, which is a feature of increasing interest for several applications, including wireless power transfer, medical imaging, as well as buried-object detection and secure communications. Thanks to its simplicity and wideband nature, the antenna represents a possible alternative to both RLSA designs, which are based on the deployment of a great number of discrete slots, and to more resonant designs.

Thanks also to the very large operative fractional bandwidth, by controlling the inherent dispersive behavior of this class of backward LW antennas, unprecedented possibilities are possible in the field of the polychromatic synthesis and characterization of nondiffracting waves in the microwave and millimeter-wave ranges. Future work can also include exploring the far-field response for the proposed LWA. In that this class of LWA could be useful for Bessel beam generation in the near-field over a large operating bandwidth, and more conventional frequency beam scanning in the far-field. This defines a dual functional antenna, and to our knowledge, such a topic has not been researched previously.

Acknowledgment

This project has received funding from the European Union's Horizon 2020 research and innovation programme under the Marie Sklodowska-Curie grant agreement No 709372. Also, the authors would like to indicate that the work is only the authors' views, and that the Horizon 2020 Agency is not responsible for any information contained in the paper.

References

[1] J. Durnin, "Exact solutions for nondiffracting beams. i. the scalar theory," *J. Opt. Soc. Am. A*, vol. 4, no. 4, pp. 651–654, 1987.
[2] H. E. Hernández-Figueroa, M. Zamboni-Rached, and E. Recami, *Non-diffracting Waves*. John Wiley & Sons, 2013.
[3] J. Durnin, J. J. Miceli Jr., and J. H. Eberly, "Diffraction-free beams," *Phys. Rev. Lett.*, vol. 58, no. 15, pp. 1499–1501, 1987.
[4] S. Mishra, "A vector wave analysis of a Bessel beam," *Opt. Commun.*, vol. 85, no. 2, pp. 159–161, 1991.
[5] M. Lapointe, "Review of non-diffracting Bessel beam experiments," *Opt. Laser Technol.*, vol. 24, no. 6, pp. 315–321, 1992.
[6] S. Chávez-Cerda, "A new approach to Bessel beams," *J. Mod. Opt.*, vol. 46, no. 6, pp. 923–930, 1999.
[7] D. McGloin and K. Dholakia, "Bessel beams: diffraction in a new light," *Contemp. Phys.*, vol. 46, no. 1, pp. 15–28, 2005.
[8] Z. Li, K. B. Alici, H. Caglayan, and E. Ozbay, "Generation of an axially asymmetric Bessel–like beam from a metallic subwavelength aperture," *Phys. Rev. Lett.*, vol. 102, p. 143901, Apr 2009.

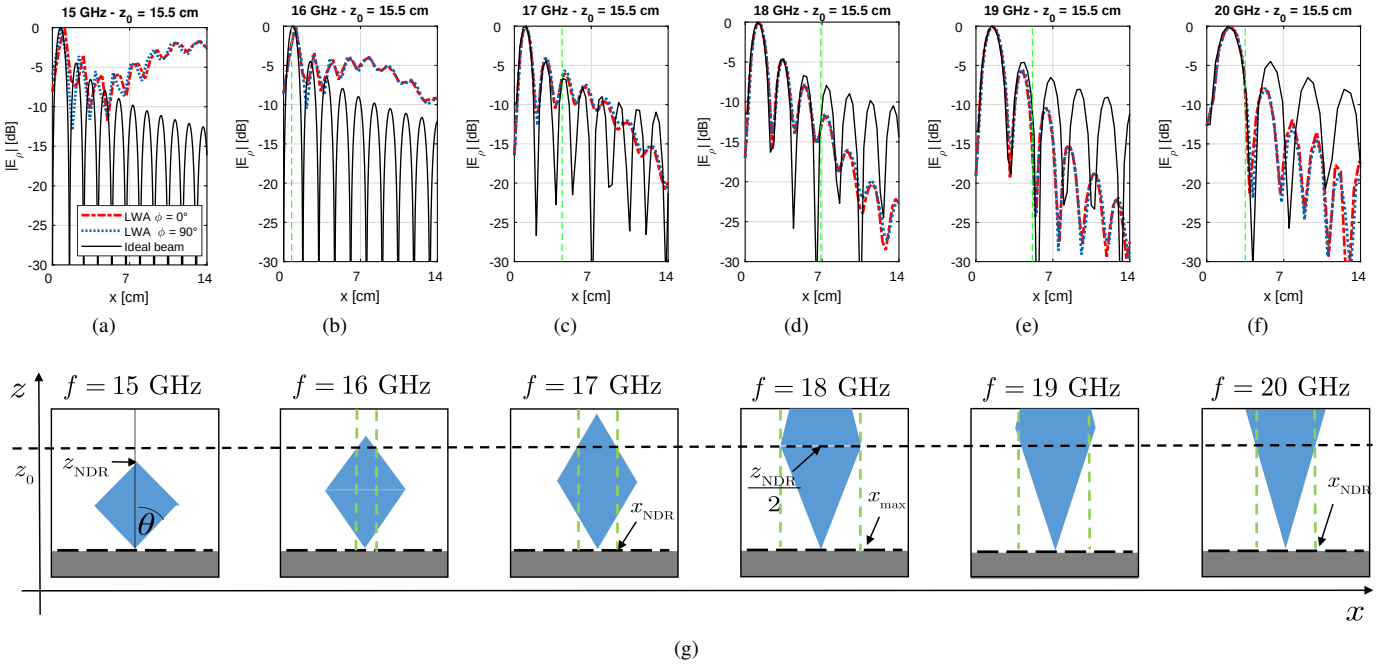

Fig. 17. 1-D profile of the electric field on the plane $z = z_0 = 15.5$ cm parallel to the aperture along $\phi = 0°$ and $\phi = 90°$: comparison between measurements (red dashed-dotted lines, $\phi = 0°$; blue dashed lines, $\phi = 90°$) and an ideal Bessel beam produced by an infinite aperture (black solid line). (a) from $f = 15$ GHz to (f) $f = 20$ GHz. The relevant values of the NDR for each frequency can be obtained by inspection of Fig. 18. It should be mentioned that the same xy plane has been considered for the six values of frequency. Hence the sub-figures (a) and (b) report two radial cuts that are outside and on the boundary of the relevant NDR (z_{NDR} equal to about 11 cm and 16 cm, respectively). For this reason, it can be observed that the near-field starts to diffract. It is important to highlight the transition from a collimated beam to a slightly diffracted beam. It should be noted that there is a good agreement between a Bessel-beam profile and the measurements within the predicted radial extent x_{NDR} of the nondiffractive region (denoted by the vertical green dashed line. g) Evolution of the nondiffractive region (in blue) as the frequency increases. Due to the dispersive behavior of β_{-1}/k_0 (see Fig. 18), the angle θ decreases with frequency, thus closing the shadow boundaries and extending the nondiffractive range farther. Since the measurements are shown at the fixed vertical distance from the aperture $z_0 = 15.5$ cm, the measured 1-D profiles are expected to agree with an ideal Bessel beam profile up to a radial distance which changes with frequency and is here delimited by the vertical dashed green lines.

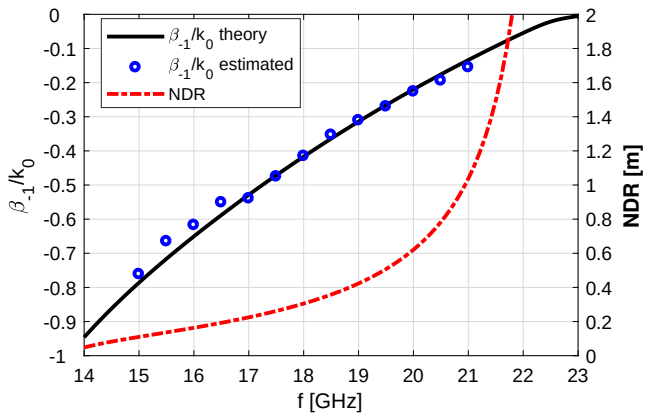

Fig. 18. Estimated phase constant from the measured beams (left axis) and dispersive behavior of the nondiffracting range (right axis). The values of the estimated LW phase constant were determined using a horizontal observational plane $z = z_0$ inside the NDR (where, indeed, the beam is a Bessel beam). Specifically at $z_0 = \mathrm{NDR}(f_0)/2$ for frequencies from $f = 15$ to 16.5 GHz, and at $z_0 = 15.5$ cm for the all other cases, as in Fig. 17.

[9] M. A. Salem, A. H. Kamel, and E. Niver, "Microwave Bessel beams generation using guided modes," *IEEE Trans. Antennas Propag.*, vol. 59, no. 6, pp. 2241–2247, 2011.

[10] M. Ettorre and A. Grbic, "Generation of propagating Bessel beams using leaky-wave modes," *IEEE Trans. Antennas Propag.*, vol. 60, no. 8, pp. 3605–3613, 2012.

[11] M. Ettorre, S. M. Rudolph, and A. Grbic, "Generation of propagating Bessel beams using leaky-wave modes: experimental validation," *IEEE Trans. Antennas Propag.*, vol. 60, no. 6, pp. 2645–2653, 2012.

[12] P. Lemaitre-Auger, S. Abielmona, and C. Caloz, "Generation of Bessel beams by two-dimensional antenna arrays using sub-sampled distributions," *IEEE Trans. Antennas Propag.*, vol. 61, no. 4, pp. 1838–1849, 2013.

[13] C. Pfeiffer and A. Grbic, "Controlling vector Bessel beams with metasurfaces," *Phys. Rev. App.*, vol. 2, no. 4, p. 044012, 2014.

[14] M. Ettorre, M. Casaletti, G. Valerio, R. Sauleau, L. Le Coq, S. C. Pavone, and M. Albani, "On the near-field shaping and focusing capability of a radial line slot array," *IEEE Trans. Antennas Propag.*, vol. 62, no. 4, pp. 1991–1999, 2014.

[15] A. Mazzinghi, M. Balma, D. Devona, G. Guarnieri, G. Mauriello, M. Albani, and A. Freni, "Large depth of field pseudo–Bessel beam generation with a RLSA antenna," *IEEE Trans. Antennas Propag.*, vol. 62, no. 8, pp. 3911–3919, 2014.

[16] Y. C. Zhong and Y. J. Cheng, "Ka-band wideband large depth-of-field beam generation through a phase shifting surface antenna," *IEEE Trans. Antennas Propag.*, vol. 64, no. 12, pp. 5038–5045, Dec 2016.

[17] W. Fuscaldo, G. Valerio, A. Galli, R. Sauleau, A. Grbic, and M. Ettorre, "Higher-order leaky-mode Bessel-beam launcher," *IEEE Trans. Antennas Propag.*, vol. 64, no. 3, pp. 904–913, Mar. 2016.

[18] M. Albani, S. Pavone, M. Casaletti, and M. Ettorre, "Generation of non-diffractive Bessel beams by inward cylindrical traveling wave aperture distributions," *Opt. Express*, vol. 22, no. 15, pp. 18 354–18 364, 2014.

[19] M. Ettorre, S. C. Pavone, M. Casaletti, and M. Albani, "Experimental validation of Bessel beam generation using an inward Hankel aperture distribution," *IEEE Trans. Antennas Propag.*, vol. 63, no. 6, June 2015.

[20] S. C. Pavone, M. Ettorre, and M. Albani, "Analysis and design of Bessel beam launchers: Longitudinal polarization," *IEEE Trans. Antennas Propag.*, vol. 64, no. 6, pp. 2311–2318, Mar. 2016.

[21] D. Comite, G. Valerio, M. Albani, A. Galli, M. Casaletti, and M. Ettorre, "Exciting vorticity through higher-order bessel beams with a radial-line

slot-array antenna," *IEEE Trans. Antennas Propag.*, vol. 65, no. 4, pp. 2123–2128, Feb 2017.

[22] N. Kou, S. Yu, and L. Li, "Generation of high-order Bessel vortex beam carrying orbital angular momentum using multilayer amplitude-phase-modulated surfaces in radiofrequency domain," *App. Phys. Express*, vol. 10, no. 1, p. 016701, 2017.

[23] M. Q. Qi, W. X. Tang, and T. J. Cui, "A broadband Bessel beam launcher using metamaterial lens," *Sci. Rep.*, vol. 5, p. 11732, 2015.

[24] Y. C. Zhong and Y. J. Cheng, "Wideband quasi-non-diffraction beam with accurately controllable propagating angle and depth-of-field," *IEEE Trans. Antennas Propag.*, 2017, in press.

[25] B. G. Cai, Y. B. Li, W. X. Jiang, Q. Cheng, and T. J. Cui, "Generation of spatial Bessel beams using holographic metasurface," *Opt. Express*, vol. 23, no. 6, pp. 7593–7601, 2015.

[26] J. L. Gómez-Tornero, D. Blanco, E. Rajo-Iglesias, and N. Llombart, "Holographic surface leaky-wave lenses with circularly-polarized focused near-fields–Part I: Concept, design and analysis theory," *IEEE Trans. Antennas Propag.*, vol. 61, no. 7, pp. 3475–3485, Apr. 2013.

[27] D. Blanco, J. L. Gmez-Tornero, E. Rajo-Iglesias, and N. Llombart, "Holographic surface leaky-wave lenses with circularly-polarized focused near-fields–Part II: Experiments and description of frequency steering of focal length," *IEEE Trans. Antennas Propag.*, vol. 61, no. 7, pp. 3486–3494, July 2013.

[28] A. J. Martinez-Ros, J. L. Gómez-Tornero, V. Losada, F. Mesa, and F. Medina, "Non-uniform sinusoidally modulated half-mode leaky-wave lines for near-field focusing pattern synthesis," *IEEE Trans. Antennas Propag.*, vol. 63, no. 3, pp. 1022–1031, Dec. 2015.

[29] D. R. Jackson and A. A. Oliner, "Leaky-wave antennas," in *Modern Antenna Handbook*, C. A. Balanis, Ed. Hoboken, NJ, USA: John Wiley & Sons, 2008, ch. 7, pp. 325–367.

[30] S. K. Podilchak, P. Baccarelli, P. Burghignoli, A. P. Freundorfer, and Y. M. Antar, "Optimization of a planar "Bull-eye" leaky–wave antenna fed by a printed surface–wave source," *IEEE Antennas and Wireless Propagation Letters*, vol. 12, pp. 665–669, 2013.

[31] ——, "Analysis and design of annular microstrip-based planar periodic leaky-wave antennas," *IEEE Trans. Antennas Propag.*, vol. 62, no. 6, pp. 2978–2991, 2014.

[32] D. Comite, S. K. Podilchak, P. Baccarelli, P. Burghignoli, A. Galli, A. P. Freundorfer, and Y. M. M. Antar, "A dual-layer planar leaky-wave antenna designed for linear scanning through broadside," *IEEE Antennas Wireless Propag. Lett.*, vol. 16, pp. 1106–1110, 2017.

[33] A. Ip and D. R. Jackson, "Radiation from cylindrical leaky waves," *IEEE Trans. Antennas Propag.*, vol. 38, no. 4, pp. 482–488, 1990.

[34] S. C. Pavone, A. Mazzinghi, A. Freni, and M. Albani, "Comparison between broadband bessel beam launchers based on either bessel or hankel aperture distribution for millimeter wave short pulse generation," *Opt. Express*, vol. 25, no. 16, pp. 19 548–19 560, Aug 2017.

[35] A. Mazzinghi and A. Freni, "Simultaneous generation of pseudo–Bessel vortex modes with a RLSA," *IEEE Antennas Wireless Propag. Lett.*, vol. 16, pp. 1747–1750, 2017.

[36] E. Mari, F. Spinello, M. Oldoni, R. A. Ravanelli, F. Romanato, and G. Parisi, "Near-field experimental verification of separation of OAM channels," *IEEE Antennas Wireless Propag. Lett.*, vol. 14, pp. 556–558, 2015.

[37] D. Comite, W. Fuscaldo, P. Burghignoli, P. Baccarelli, S. K. Podilchak, and A. Galli, "Bessel beam generation by means of annular leaky–wave antennas," in *Proc. 11th European Conf. Antennas Propag.*, Mar. 2017, pp. 3863–3864.

[38] P. Baccarelli, P. Burghignoli, G. Lovat, and S. Paulotto, "A novel printed leaky–wave "bull-eye" antenna with suppressed surface–wave excitation," in *Proc. IEEE Antennas Prop. Society Symp., 2004.*, June 2004, pp. 1078–1081.

[39] P. Baccarelli, P. Burghignoli, F. Frezza, A. Galli, and P. Lampariello, "Novel modal properties and relevant scanning behaviors of phased arrays of microstrip leaky-wave antennas," *IEEE Trans. Antennas Propag.*, vol. 51, no. 12, pp. 3228–3238, Dec 2003.

[40] M. Abramowitz and I. A. Stegun, *Handbook of Mathematical Functions*. New York: Dover, 1962.

[41] P. Baccarelli, P. Burghignoli, C. Di Nallo, F. Frezza, A. Galli, P. Lampariello, and G. Ruggieri, "Full-wave analysis of printed leaky-wave phased arrays," *Int. J. RF Microwave Computer Aided Eng.*, vol. 12, no. 3, pp. 272–287, 2002.

[42] S. K. Podilchak, *Planar leaky–wave antennas and microwave circuits by practical surface wave launching*. Queen's University, Kingston, Ontario, Canada, Ph.D. Dissertation, 2013.

[43] C. A. Balanis, *Advanced Engineering Electromagnetics*. Wiley Online Library, 2012.

[44] P. Baccarelli, P. Burghignoli, F. Frezza, A. Galli, G. Lovat, and D. R. Jackson, "Approximate analytical evaluation of the continuous spectrum in a substrate-superstrate dielectric waveguide," *IEEE Trans. Microwave Theory Tech.*, vol. 50, no. 12, pp. 2690–2701, Dec 2002.